# FORMULATION OF A HIGH-FIDELITY NUCLEAR FISSION SITES CONVERGENCE DETECTION METHOD IN MONTE CARLO REACTOR SAFETY ASSESSMENTS

# **CHIN KEN FUI**

UNIVERSITI SAINS MALAYSIA

# FORMULATION OF A HIGH-FIDELITY NUCLEAR FISSION SITES CONVERGENCE DETECTION METHOD IN MONTE CARLO REACTOR SAFETY ASSESSMENTS

by

# **CHIN KEN FUI**

Thesis submitted in fulfilment of the requirements for the Degree of Master of Science

#### **ACKNOWLEDGEMENT**

I am grateful to acknowledge my supervisor, Dr Muhammad Rabie bin Omar, for providing me with the opportunity to participate in and explore this research. His guidance and insights have been invaluable throughout my journey as a master's student. I would also like to extend my appreciation to my co-supervisors, Assoc. Prof. Dr Yoon Tiem Leong and Dr Julia binti Abdul Karim, for their invaluable advice and support during this research endeavour. I would like to express my sincere gratitude to Universiti Sains Malaysia for their financial support through the Short Term Grant (No. 304/PFIZIK/6315550) and the Graduate Student Financial Assistance (GRA-ASSIST). Moreover, I would like to thank Ybhg. Prof. Ts. Dr M. Iqbal Bin Saripan and Dr Wong Khai Ming for their invaluable insights in refining this thesis. Lastly, I would like to convey my heartfelt thanks to my family and friends for their unwavering support throughout my academic journey. Their encouragement and belief in me have been instrumental in my achievements.

# TABLE OF CONTENTS

ACK	NOWLEDGEMENT	ii			
TAB	ELE OF CONTENTS	iii			
LIST	T OF TABLES	v			
LIST	Γ OF FIGURES	vi			
LIST	T OF SYMBOLS	viii			
LIST	Γ OF ABBREVIATIONS	X			
LIST	T OF APPENDICES	xi			
ABS	TRAK	xii			
ABS	TRACT	xiv			
CHA	APTER 1 INTRODUCTION	1			
1.1	Background	1			
1.2	Problem Statement				
1.3	Objectives4				
1.4	Scope and Limitations 4				
1.5	Thesis Outline6				
CHA	APTER 2 THEORY AND LITERATURE REVIEW	7			
2.1	Neutron Transport Equation	7			
	2.1.1 Time-Independent Form and Multiplication Factor	10			
	2.1.2 Standard Power Iteration	12			
2.2	Nuclear Criticality Calculation	14			
	2.2.1 The Monte Carlo Method	14			
	2.2.2 Monte Carlo Criticality Calculation	18			
2.3	Source Convergence Indicators	19			
	2.3.1 Entropy-Based Indicators	20			
	2.3.2 Mesh-Free Indicators	23			

	2.3.3 Source Convergence Instance Diagnostics				
	2.3.4 Summary and Motivation	. 31			
СНА	PTER 3 METHODOLOGY	. 33			
3.1	Fourier Fundamental Mode Coefficient	. 33			
3.2	One-Dimensional Fourier Fundamental Mode Coefficients				
3.3	OpenMC4				
3.4 Computational Models		. 45			
	3.4.1 Simple Homogeneous Reactor Model	. 46			
	3.4.2 OECD/NEA Checkerboard Benchmark Problem	. 48			
	3.4.3 3D BEAVRS Full Core Model	. 50			
CHAI	PTER 4 RESULTS AND DISCUSSIONS	. 52			
4.1	Simple Homogeneous Reactor Model	. 52			
4.2	OECD/NEA Benchmark Problem: Checkerboard Storage of Assemblies	. 66			
4.3	3D BEAVRS Full Core Model	. 79			
4.4	Summary and Limitations	. 90			
CHAI	PTER 5 CONCLUSION AND RECOMMENDATIONS	. 91			
5.1	Conclusion	. 91			
5.2	Recommendations and Future Works	. 92			
REFE	CRENCES	. 93			
APPE	ENDICES				
LIST	OF PUBLICATIONS				

# LIST OF TABLES

	Page
Table 4.1	Bounding enclosures of FFMC for the simple rectangular cuboid homogeneous reactor
Table 4.2	Bounding enclosures of FFMC for the simple cube homogeneous reactor
Table 4.3	Material compositions for checkerboard storage of fuel assemblies 68
Table 4.4	Pearson correlation coefficients $(R)$ between WD and 1D-FFMC with a uniform initial source distribution across all fuel assemblies under different neutron histories per cycle $(N)$ for the checkerboard storage of fuel assemblies benchmark problem
Table 4.5	Performance evaluation of WD and 1D-FFMC with a uniform initial source distribution across all fuel assemblies under different neutron histories per cycle $(N)$ for the checkerboard storage of fuel assemblies benchmark problem.
Table 4.6	Pearson correlation coefficients ( <i>R</i> ) between WD and 1D-FFMC with a uniform initial source distribution across the fuel assembly (1, 3) under different neutron histories per cycle ( <i>N</i> ) for the checkerboard storage of fuel assemblies benchmark problem
Table 4.7	Performance evaluation of WD and 1D-FFMC with a uniform initial source distribution across the fuel assembly (1, 3) under different number of neutron histories per cycle (N) for the checkerboard storage of fuel assemblies benchmark problem
Table 4.8	Axial specification of 3D BEAVRS fuel rod pin cell
Table 4.9	Pearson correlation coefficients of WD and 1D-FFMC for the 3D BEAVRS full core model
Table 4.10	Performance evaluation of WD and 1D-FFMC for the 3D BEAVRS full core model.

# LIST OF FIGURES

	Page
Figure 2.1	The values of $\pi$ estimated by the Monte Carlo method under different numbers of points $P$
Figure 2.2	The Monte Carlo calculation flowchart for estimating the value of $\pi$ .
Figure 2.3	The Wasserstein distance (WD) calculation flowchart. The caret symbol (^) indicates additional modifications to the standard MC algorithm
Figure 3.1	The FFMC calculation flowchart. The asterisk (*) symbol indicates additional modifications to the standard MC algorithm
Figure 3.2	Geometry of the OECD/NEA benchmark problem: checkerboard storage of fuel assemblies
Figure 4.1	Evolution of source fractions along three Cartesian axes for the simple rectangular cuboid homogeneous reactor
Figure 4.2	Convergence plots of normalized FFMC under varied sizes of bounding enclosures for the simple rectangular cuboid homogeneous reactor
Figure 4.3	Convergence plots of normalized 1D-FFMC under varied sizes of bounding enclosures for the simple rectangular cuboid homogeneous reactor
Figure 4.4	Evolution of source fractions along the three Cartesian axes for the simple cube homogeneous reactor
Figure 4.5	Convergence plots of normalized FFMC under varied sizes of bounding enclosures for the simple cube homogeneous reactor
Figure 4.6	Convergence plots of normalized 1D-FFMC under varied sizes of bounding enclosures for the simple cube homogeneous reactor65
Figure 4.7	Geometry of the OECD/NEA benchmark problem: checkerboard storage of fuel assemblies
Figure 4.8	Convergence plots of 1D-FFMC and WD with a uniform initial source distribution across all fuel assemblies under 25,000 neutron histories per cycle for the checkerboard storage of fuel assemblies benchmark problem

Figure 4.9	Convergence plots of normalized 1D-FFMC with a uniform initial source distribution across all fuel assemblies under different neutron histories per cycle (N) for the checkerboard storage of fuel assemblies benchmark problem
Figure 4.10	Convergence plots of WD with a uniform initial source distribution across all fuel assemblies under different neutron histories per cycle (N) for the checkerboard storage of fuel assemblies benchmark problem
Figure 4.11	Convergence plots of 1D-FFMC and WD with a uniform initial source distribution across the fuel assembly (1, 3) under 25,000 neutron histories per cycle for the checkerboard storage of fuel assemblies benchmark problem.
Figure 4.12	Convergence plots of normalized 1D-FFMC with a uniform initial source distribution across the fuel assembly $(1, 3)$ under different neutron histories per cycle $(N)$ for the checkerboard storage of fuel assemblies benchmark problem.
Figure 4.13	Convergence plots of WD with a uniform initial source distribution across the fuel assembly (1, 3) under different neutron histories per cycle (N) for the checkerboard storage of fuel assemblies benchmark problem
Figure 4.14	Geometry of the 3D BEAVRS full core model
Figure 4.15	Horizontal cross section of the fuel assembly lattice at the elevation of 257.4735 cm with an origin at (0, 21.5036) cm for the 3D BEAVRS full core model
Figure 4.16	Convergence plots of 1D-FFMC and WD with the first random seed for the 3D BEAVRS full core model
Figure 4.17	Convergence plots of 1D-FFMC and WD with the second random seed for the 3D BEAVRS full core model
Figure 4.18	Convergence plots of 1D-FFMC and WD with the third random seed for the 3D BEAVRS full core model
Figure 4.19	Convergence plots of 1D Fourier coefficients with the first random seed for the 3D BEAVRS full core model
Figure 4.20	Convergence plots of 1D Fourier coefficients with the second random seed for the 3D BEAVRS full core model
Figure 4.21	Convergence plots of 1D Fourier coefficients with the third random seed for the 3D BEAVRS full core model

# LIST OF SYMBOLS

$c_f$	Fourier fundamental mode coefficient
$c_{f\alpha}$	One-dimensional Fourier fundamental mode coefficient along $\alpha$ direction
E	Energy
F	Fission multiplication operator
H	Shannon entropy
$k_{ m eff}$	Effective multiplication factor
L	Leakage operator
N	Number of neutron histories per cycle
n	Neutron density
$N_D$	Atomic density
$N_F$	Number of fission sites generated
Q	Change of neutron population from production or absorption events
R	Pearson correlation coefficient
$\vec{r}$	Position vector
S	In-scattering operator
t	Time
T	Total absorption operator
V	Volume
υ	Neutron speed
$\mathrm{WD}_lpha$	Wasserstein distance measure along $\alpha$ direction
$\mathbb{Z}$	Set of integers $\{, -2, -1, 0, 1, 2,\}$
$\nu(E)$	Average number of neutrons produced per fission by incident energy $E$
$\Sigma_f$	Macroscopic fission cross section

- $\Sigma_s$  Double-differential scattering cross section
- $\Sigma_t$  Macroscopic total cross section
- $\chi(E)$  Fission spectrum for neutron with ejected energy E
- Ψ Fission source distribution
- $\psi$  Neutron flux
- $\widehat{\Omega}$  Unit vector in direction of motion

# LIST OF ABBREVIATIONS

1D-FFMC One-dimensional Fourier fundamental mode coefficient

3D Three-dimensional Form

BEAVRS Benchmark for evaluation and validation of reactor simulations

cm centimetre

FFMC Fourier fundamental mode coefficient

MC Monte Carlo

MIT Massachusetts Institute of Technology

NEA Nuclear Energy Agency

OECD Organisation for Economic Co-operation and Development

U-235 Uranium-235

UO<sub>2</sub> Uranium dioxide

WD Wasserstein distance

# LIST OF APPENDICES

Appendix A XML File for Material Data of 3D BEAVRS Full Core Model

Appendix B XML File for Geometry Data of 3D BEAVRS Full Core Model

# FORMULASI KAEDAH PENGESANAN KONVERGENSI TAPAK PEMBELAHAN NUKLEAR FIDELITI TINGGI DALAM PENILAIAN KESELAMATAN REAKTOR MONTE CARLO

#### **ABSTRAK**

Simulasi pengangkutan neutron Monte Carlo (MC) merupakan alat pengiraan yang digunakan secara luas untuk menilai keselamatan pelbagai teknologi nuklear, termasuk reaktor nuklear. Semasa simulasi tersebut, tekaan awal taburan sumber neutron diperlukan, dan apabila beberapa kitaran MC disimulasikan, ia akan menumpu kepada taburan sebenar secara beransuran. Hasil daripada beberapa kitaran awal dibuang, dan hasil daripada kitaran seterusnya dikumpul untuk mendapatkan keputusan yang bermakna secara statistik. Oleh itu, pengenalpastian trend penumpuan dengan tepat adalah penting untuk mengelakkan pengumpulan ralat yang berpunca daripada tekaan awal. Teknik diagnostik penumpuan tradisional bergantung kepada pendiskretan geometri masalah, dan prestasi serta ketepatannya sering dipengaruhi oleh skema jejaring yang dipilih. Dalam penyelidikan ini, penunjuk diagnostik penumpuan yang bebas jejaring dan baharu, namanya pekali mod asas Fourier (FFMC), dirumus dan diperhalusi. Kaedah FFMC menggunakan pengembangan siri Fourier pada tapak pembelahan, dan aruhan matematik menunjukkan mod asas bagi pekali Fourier mempamerkan penumpuan yang paling perlahan apabila taburan sumber neutron menumpu. Pelaksanaan kaedah FFMC dengan algoritma MC piawai adalah mudah. Untuk menangani kelemahan kaedah FFMC, kebolehgunaan FFMC dikaji dalam konteks model reaktor homogen mudah. Penambahbaikan ini membawa kepada pembangunan pekali satu dimensi, yang dirujuk sebagai 1D-FFMC. Cadangan

kepungan yang berbatasan untuk 1D-FFMC ialah peliputan kawasan fisi yang tepat. Tujuannya untuk memastikan perwakilan sistem yang tepat. Kesahihan kaedah 1D-FFMC diujikan dengan membandingkannya dengan penunjuk jarak Wasserstein (WD) yang baharu dalam masalah penanda aras simpanan papan dam dan model penuh 3D BEAVRS. Kedua-dua penunjuk menunjukkan persetujuan yang tinggi dari segi hasil penumpuan, dengan kaedah 1D-FFMC menunjukkan kecekapan pengiraan yang dipertingkatkan, sekurang-kurangnya 17% lebih cepat daripada kaedah WD.

# FORMULATION OF A HIGH-FIDELITY NUCLEAR FISSION SITES CONVERGENCE DETECTION METHOD IN MONTE CARLO REACTOR SAFETY ASSESSMENTS

#### **ABSTRACT**

Monte Carlo (MC) neutron transport simulation is a widely used computational tool for assessing the safety of various nuclear technologies, including nuclear reactors. During the simulation, an initial guess of the neutron source distribution is required, and as several MC cycles are simulated, it converges to the true distribution. The outcomes from the initial cycles are discarded, and the outcomes from the subsequent cycles are accumulated to obtain a statistically meaningful result. Therefore, accurately identifying the convergence trend is crucial to prevent error accumulation from the initial guess. Traditional convergence diagnostic techniques rely on discretizing the problem geometry, and the selected meshing scheme heavily influences their performance and accuracy. This research formulated and refined a novel mesh-free convergence diagnostic indicator called Fourier fundamental mode coefficient (FFMC). The FFMC method utilizes the Fourier series expansion on the fission sites, and the mathematical induction shows that the fundamental mode of the Fourier coefficient exhibits the slowest convergence as the neutron source distribution converges. Implementing the FFMC method with a standard MC algorithm is straightforward. The limitations of the FFMC method are assessed and refined in the context of a simple homogenous reactor model. This refinement leads to onedimensional coefficients, referred to as 1D-FFMC. Regarding the bounding enclosure for 1D-FFMC, it is recommended to enclose the fissile region exactly, ensuring an

accurate neutron source distribution representation. The validity of the 1D-FFMC method is verified by comparing it with the stage-of-the-arts Wasserstein distance (WD) indicator using the checkerboard storage of fuel assemblies benchmark problem and the 3D BEAVRS full core model. Both indicators exhibit high agreement in terms of convergence results, with the 1D-FFMC method demonstrating enhanced computational efficiency, being at least 17% faster than the WD method.

#### **CHAPTER 1**

#### INTRODUCTION

## 1.1 Background

Nowadays, the energy consumption by the current population is tremendous due to modernization and digitalization. As we advance towards the Fourth Industrial Revolution or the Age of Imagination, electrical energy becomes crucial for new-age technologies such as the Internet of Things, artificial intelligence, cloud computing, and other related domains. Electricity is generated from various primary energy sources, including fossil fuels, mineral fuels, biomass, solar energy, wind energy, geothermal energy, and others. However, using conventional energy sources such as fossil fuels, including coal, oil, and gas, negatively impacts our environment and society. For instance, burning fossil fuels releases carbon dioxide, contributing to the greenhouse effect. Thus, there is a demand for a shift towards using green energy to ensure the sustainability of human activities. Among other green energy sources, nuclear energy emerges as a potential substitute for fossil fuels. Due to the enormous energy released per unit of fuel through fission or fusion reactions, nuclear reactions are preferred to chemical burning reactions. Currently, only fission reactors are commercially available, while fusion reactors are still in the research stage. It is crucial to ensure the safety of fission reactors, as a failure in the safety assessment of fission reactors could result in a disaster, as seen in the Fukushima and Chernobyl accidents. The safety of a nuclear power system can be assessed through experiments or computational simulation. Computational simulation is preferred over experiments due to its flexibility to scale up and its low cost of operation. The reliability of the simulation depends on the accuracy and consistency of the numerical methods used. The neutron transport equation describes the behaviour of the nuclear reactor core, and solving it reveals the stability of the nuclear reactor. The equation can be solved using two numerical methods: the deterministic method and the Monte Carlo method. The Monte Carlo simulation is currently preferred due to the availability of high-performance computing and its capability to simulate various complex geometries.

#### 1.2 Problem Statement

In Monte Carlo (MC) neutron transport simulation, the neutron distribution inside a fissile system can be obtained from an initial guess distribution by simulating each neutron from its birth to its termination. The initial guess neutron distribution consists of N locations, where N represents the input parameter for the number of simulated neutrons. Each location serves as the starting point, from which the neutron begins its random transport within the fissile system until its termination location. During the transport, the neutron may undergo various reactions such as scattering, capture, or fission events, which depend on a set of random numbers and the cross sections of the materials. Once all neutrons have been simulated, an MC cycle or generation is considered complete. The termination locations resulting from the fission event are assigned as the birth locations for the subsequent MC cycle. These locations are known as the fission sites. The number of fission sites in the next cycle may differ from the number of simulated neutrons, so the fission site count is normalized to N. This normalization is performed to prevent an exponential increase or decrease in the number of neutrons, which could lead to premature termination of the simulation. As more cycles are simulated, the neutron distribution fluctuates and eventually converges to a stationary or equilibrium state. Tally quantities such as power distribution and reaction rates can only be accumulated once equilibrium has been achieved to avoid

errors arising from the initial guess. The iteration process is divided into inactive cycles for the purpose of convergence and active cycles for the tally of quantities of interest. False convergence detection in nuclear systems could lead to a catastrophic nuclear accident. Hence, it is crucial to improve the reliability of the convergence method to avoid critical errors in assessing the safety of a fissile system.

To ensure the safety of a nuclear system, the convergence of neutron distribution must be realized before collecting the tallied results, ensuring that the results are free from contamination due to an incorrect estimation of the initial distribution (Kumar et al., 2020; Srivastava et al., 2020; Yamamoto & Sakamoto, 2020). The conventional approach to address this challenge involves using an indicator to characterize the change in the distribution across successive MC cycles. However, the traditional convergence indicator is less precise and computationally expensive as it requires discretizing the problem space into a mesh comprising small bins. The fluctuations of the neutron source distribution are averaged by the summation over each mesh, which is likely to overlook any local changes in a smaller region (Kumar et al., 2020; Nowak et al., 2016). Moreover, the choice of the space discretization scheme is subjective, with different problems requiring different schemes, making the diagnosis of stationarity more challenging (Kumar et al., 2020; Omar, 2021a; Ueki & Chapman, 2011). Also, an excessively high or low discretization may fail to reveal details changes in the neutron source distribution (Brown et al., 2007; Cheatham & Brown, 2006). Therefore, a novel method is required to overcome the limitations of conventional approach by eliminating the need for space discretization. This proposed method must undergo validation with various reactor models and offers advantages in terms of implementation, computational efficiency, and adaptability to various reactor geometries.

# 1.3 Objectives

The general objective of this research is to formulate a mesh-free or no spatial discretization mathematical technique for detecting the convergence of fission sites in Monte Carlo simulation for nuclear reactor safety assessment. Two sub-objectives that contribute to the achievement of the main objective are listed as follows:

- 1. The first sub-objective aims to model the nuclear reactors and use the models to validate the proposed method.
- 2. The second sub-objective aims to propose a simplified solution which enhances ease of implementation, computational efficiency, and adaptability to various reactor geometries.

# 1.4 Scope and Limitations

In this study, we utilized the OpenMC code (Romano et al., 2015) for all Monte Carlo (MC) neutron transport simulations. We expect that other MC codes would lead to the same conclusions as this study. These simulations include three models: a simple homogeneous reactor model, a checkerboard benchmark problem, and a 3D full core reactor model. For the simple homogeneous reactor model, we generated the multigroup cross section library by specifying the cross sections for various neutron-nuclear interactions. For the benchmark problem and the full core reactor model, we used continuous energy nuclear data from the ENDF/B-VIII.0 library for the target materials. Similar conclusions are expected when using other nuclear libraries.

Furthermore, OpenMC employs survival biasing as a variance reduction technique. Survival biasing is applied with a weight cutoff and Russian roulette. The weight of a neutron is adjusted by two parameters,  $w_c$  and  $w_s$ . After a collision, if the

neutron's weight w is less than  $w_c$ , it is killed with a probability of  $1 - w/w_s$ . If it survives, its weight is set to  $w_s$ . In OpenMC, the cutoff weight is set as  $w_c = 0.25$  and  $w_s = 1.0$ . It should be noted that different MC codes may use different variance reduction techniques, which should not pose any major issue.

Additionally, Python was used to calculate the Pearson coefficients and evaluate performance during validation. All simulations and calculations in this study were conducted on a Windows Subsystem for Linux (WSL) laptop equipped with an Intel Core i7-7700HQ CPU, utilizing 8 parallel processes. This computational capacity allowed for simulations of up to 1 million neutron histories per MC cycle with an appropriate simulation duration. It is important to acknowledge that the results of performance assessment may differ based on the choice of programming languages, operating systems, and computational hardware used in the study.

This research introduces a novel method for source convergence detection, characterized by its high efficiency and ease of implementation within standard MC codes. The nuclear community, particularly the Malaysian Nuclear Agency, can benefit from cost savings by avoiding licensing fees for MC codes and high-performance computing. This method greatly integrates with the free and open-source code, OpenMC, while requiring fewer computing resources compared to other available methods. However, the primary challenge in disseminating the ideas of this project within the nuclear community is convincing them to adopt and test this method for various nuclear problems and models. The community can be conservative, making it challenging to persuade them to switch to a new method, as it may disrupt their existing processes.

#### 1.5 Thesis Outline

This thesis comprises five chapters: introduction, theory and literature review, methodology, results and discussions, and conclusion. **Chapter one** provides the background of the research, the problem statement, the research objectives, and the thesis outline. **Chapter two** discusses the relevant theory for this research, specifically the neutron transport equation and the Monte Carlo criticality calculation. This chapter also summarizes the previous research that addressed the same research problem: proposing new methods to determine the convergence of neutron source distribution. **Chapter three** presents the formulation of a new convergence detection method based on Fourier series expansion. The Fourier method is improved by dissociating it into three one-dimensional indicators. **Chapter four** highlights the erroneous convergence results of the proposed method for a simple homogeneous reactor model, emphasizing the need for an improved indicator. The improved indicator is validated by a benchmark problem and a real reactor model to establish its reliability and efficiency in determining stationarity. Finally, **chapter five** summarizes the findings that address the research problem and suggests perspectives to advance the research field.

#### **CHAPTER 2**

#### THEORY AND LITERATURE REVIEW

This chapter elucidates the theory behind this research, from the fundamental principles to the novel concept. The neutron transport equation is initially derived based on intuitive ideas, followed by its time-independent form, and further developed into nuclear criticality calculation. The nuclear criticality problem can be addressed using the Monte Carlo numerical method, which is explained in detail, from its fundamental concept to its application to criticality calculation. Lastly, a review of the previous methods proposed by several researchers for diagnosing the stationarity of fission sources is outlined in the last section.

# 2.1 Neutron Transport Equation

In a fissile system, the behaviour of neutrons is governed by the neutron transport equation or Boltzmann equation (Bell & Glasstone, 1970). This equation describes the motions and interactions between neutrons and nuclei but neglects the neutron-neutron interactions since the neutron density is negligible compared to the density of the materials. The main idea is to obtain the neutron population inside a specific system, treating the neutron population as a continuum. Initially, based on intuition, the conservation equation states that:

$$\frac{d}{dt} \int_{V} n \, d\tau = \int_{V} \left(\sum_{i} Q_{i}\right) d\tau$$
The substantial derivative of neutron population in a volume  $V$ 
The sum of all sources and sinks in that volume

(2.1)

where  $n = n(\vec{r}, E, \hat{\Omega}, t)$  represents the neutron density,  $Q_i$  denotes any production or absorption events of neutrons, and  $d\tau$  is a differential volume element. Also note that

 $n(\vec{r}, E, \hat{\Omega}, t) d\tau dE d\Omega$  represents the expected number of neutrons in a volume element  $d\tau$  about  $\vec{r}$ , travelling in the cone of direction  $d\Omega$  about vector  $\hat{\Omega}$ , with energies between E and E + dE, at time t. Next, the Reynolds transport theorem states that:

$$\frac{d}{dt} \int_{V} n \, d\tau = \int_{V} \frac{\partial n}{\partial t} d\tau + \int_{S} n\vec{v} \cdot d\vec{a}$$
 (2.2)

Here,  $\vec{v} = \vec{v}(E)$  denotes the neutron velocity with energy E and  $d\vec{a}$  is a differential vector surface element of the surface S. The left-hand side of Eq. (2.1) is replaced by Eq. (2.2), and the surface integral in Eq. (2.2) is transferred to the right-hand, resulting in:

$$\int_{V} \frac{\partial n}{\partial t} d\tau = \int_{V} \left( \sum_{i} Q_{i} \right) d\tau - \int_{S} n\vec{v} \cdot d\vec{a}$$
 (2.3)

Utilizing the Gauss divergence theorem, the surface integral is replaced by the volume integral:

$$\int_{V} \frac{\partial n}{\partial t} d\tau = \int_{V} \left( \sum_{i} Q_{i} \right) d\tau - \int_{V} \nabla \cdot (n\vec{v}) d\tau \tag{2.4}$$

implying:

$$\left\{ \begin{array}{l}
 \text{Rate of change of } \\
 \text{neutron population in } V
 \end{array} \right\} = \left\{ \begin{array}{l}
 \text{Rate of production of } \\
 \text{neutrons in } V
 \end{array} \right\} - \left\{ \begin{array}{l}
 \text{Rate of absorption of } \\
 \text{neutrons in } V
 \end{array} \right\}$$

$$- \left\{ \begin{array}{l}
 \text{Rate of leakage of } \\
 \text{neutrons from } V
 \end{array} \right\}$$
(2.5)

In general, neutron production events can include in-scattering or fission events. In contrast, neutron absorption events can involve any neutron loss events except leakage, such as scattering, capture, or other disappearance reactions. It is convenient to use the

angular neutron flux  $\psi = \psi(\vec{r}, E, \hat{\Omega}, t)$  to represent the neutron population by substituting the neutron density n with  $\psi = nv$ , where v = v(E) is the neutron speed with energy E. By omitting the volume integration in Eq. (2.4) and expressing the production events and the total absorption events mathematically, we obtain the following:

$$\frac{1}{v}\frac{\partial\psi}{\partial t} = \int_{\widehat{\Omega}'} \int_{E'} \Sigma_s \psi \ dE' d\Omega' + \frac{\chi}{4\pi} \int_{\widehat{\Omega}'} \int_{E'} v \Sigma_f \psi \ dE' d\Omega' - \Sigma_t \psi - \widehat{\Omega} \cdot \nabla\psi$$
(2.6)

where  $\Sigma_s \psi \ dE' d\Omega' = \Sigma_s (\vec{r}, E' \to E, \widehat{\Omega}' \to \widehat{\Omega}) \ \psi (\vec{r}, E', \widehat{\Omega}', t) \ dE' d\Omega'$  represents the expected number of in-scattered neutrons per unit length at the position  $\vec{r}$  with energy E' and travelling in the direction  $\widehat{\Omega}'$  that scatter into an energy interval dE' about E into a solid angle  $d\Omega'$  about  $\widehat{\Omega}$  at time t,

 $\frac{\chi}{4\pi} v \Sigma_f \psi \ dE' d\Omega' = \frac{\chi(E)}{4\pi} v(E') \ \Sigma_f(\vec{r}, E') \ \psi(\vec{r}, E', \widehat{\Omega}', t) \ dE' d\Omega' \quad \text{represents} \quad \text{the}$  probable number of fission neutrons produced at  $\vec{r}$  with energy with dE' about E within the cone of angles  $d\Omega'$  about  $\widehat{\Omega}$  per unit length travelled by neutron with energies E' at time t,

 $\Sigma_t \psi = \Sigma_t(\vec{r}, E) \psi(\vec{r}, E, \hat{\Omega}, t)$  represents the expected rate of absorption of neutrons at  $\vec{r}$  per unit energy per unit angle that is lost via any disappearance interactions at time t, and

 $\widehat{\Omega}\cdot \nabla \psi=\widehat{\Omega}\cdot \nabla \psi \left( \overrightarrow{r},E,\widehat{\Omega},t \right)$  represents the neutron leakage term. The production and absorption events in Eq. (2.6) are categorized into the fission (f), in-scattering (s), and total loss reactions (t) along with the specified macroscopic cross section  $\Sigma=\Sigma(\overrightarrow{r},E)$ . The macroscopic cross section is derived from the microscopic cross section  $\sigma=\sigma(\overrightarrow{r},E)$  using  $\Sigma=N_D\sigma$ , where  $N_D$  is the atom density of the interacting material, and  $\sigma$  is defined as the effective cross-sectional area per nucleus interacted by the neutrons,

which depends on the neutron position  $\vec{r}$  and energy E. The fission event is associated with two physical parameters: the fission spectrum  $\chi(E)$  and the average number of fission neutrons v(E') produced in a fission event by a neutron with energy E'. Note that  $\chi(E)$  dE represents the probability that a fission neutron will have an energy interval dE about E.

Solving Eq. (2.6) for  $\psi$  via analytic method is challenging and requires additional assumptions, such as applying Fick's law to simplify the equation. Since Eq. (2.6) is a partial differential equation, it is necessary to specify the initial and boundary conditions. Common boundary conditions include vacuum, reflective, white, and periodic conditions. When neutrons reach the vacuum boundary, they are permanently lost. The reflective boundary instructs neutrons to return as a mirror image, while the white boundary instructs neutrons to return isotropically. Neutrons crossing the periodic boundary will reappear at the opposite boundary, as both boundaries are part of a periodic lattice structure. Furthermore,  $\psi$  must be a real, finite, and non-negative function to maintain its physical interpretation.

#### 2.1.1 Time-Independent Form and Multiplication Factor

Typically, numerical methods are employed to solve the time-independent form of the neutron transport equation (Lewis & Miller, 1984). In this form, Eq. (2.6) simplifies to:

$$\widehat{\Omega} \cdot \nabla \psi + \Sigma_t \psi = \int_{\widehat{\Omega}'} \int_{E'} \Sigma_s \psi \ dE' d\Omega' + \frac{\chi}{4\pi} \int_{\widehat{\Omega}'} \int_{E'} v \Sigma_f \psi \ dE' d\Omega'$$
 (2.7)

under the assumption that boundary conditions are also time-independent.

A fissile system is considered critical if it maintains a self-sustaining, timeindependent chain reaction without external neutron sources. The system is considered supercritical or subcritical if the neutron population increases or decreases exponentially. The *effective multiplication factor*  $k_{\rm eff}$  is defined as:

$$k_{\text{eff}} = \frac{\text{Total number of neutrons born in the system}}{\text{Total number of neutrons loss in the system}}$$
 (2.8)

which characterizes the system, with  $k_{\rm eff}=1$  indicating criticality,  $k_{\rm eff}>1$  indicating supercriticality, and  $k_{\rm eff}<1$  indicating subcriticality. No general solution exists for Eq. (2.7) in supercritical or subcritical conditions since the equation is balanced in such a way that the net gain of neutrons is equal to the net loss of neutrons within the system. To address this issue, the v in Eq. (2.7) is replaced by  $v/k_{\rm eff}$ , resulting in:

$$\widehat{\Omega} \cdot \nabla \psi + \Sigma_t \psi = \int_{\widehat{\Omega}'} \int_{E'} \Sigma_s \psi \ dE' d\Omega' + \frac{1}{k_{\text{eff}}} \frac{\chi}{4\pi} \int_{\widehat{\Omega}'} \int_{E'} \nu \Sigma_f \psi \ dE' d\Omega' \tag{2.9}$$

This equation is known as the *k-eigenvalue* or *criticality equation*. By rewriting the equation into operator form, we obtain the following:

$$(\mathbf{L} + \mathbf{T})\psi = \mathbf{S}\psi + \frac{1}{k_{\text{eff}}}\mathbf{F}\psi$$
 (2.10)

where L represents the leakage operator, T represents the total absorption operator, S represents the in-scattering operator, and F represents the fission multiplication operator. Rearranging the operator yields:

$$\psi = \frac{1}{k_{\text{eff}}} (\mathbf{L} + \mathbf{T} - \mathbf{S})^{-1} \mathbf{F} \psi = \frac{1}{k_{\text{eff}}} \mathbf{R} \psi$$
 (2.11)

where  $\mathbf{R} = (\mathbf{L} + \mathbf{T} - \mathbf{S})^{-1}\mathbf{F}$ . Applying the  $\mathbf{F}$  operator to both sides results in:

$$\Psi = \frac{1}{k_{\text{eff}}} \mathbf{R} \Psi \tag{2.12}$$

where  $\Psi = \mathbf{F}\psi$  represents the fission source distribution. The general solution for the eigenvalue equation in Eq. (2.12) is given by:

$$\Psi = \sum_{i=0}^{\infty} a_i \Psi_i \tag{2.13}$$

where each eigenfunction  $\Psi_i$  corresponds to its eigenvalue  $k_i$  and expansion coefficient  $a_i$ . It is impractical to solve for a general solution. Instead, the focus is on the fundamental values of a particular system, namely  $k_0$  and  $\Psi_0$ , as  $k_0 = k_{\rm eff}$  for the system. Additionally,  $k_0$  represents the largest eigenvalue, satisfying:

$$k_0 > |k_1| > |k_2| > \cdots$$
 (2.14)

#### 2.1.2 Standard Power Iteration

Eq. (2.12) can be solved numerically using the standard power iteration method:

$$\Psi^{(j+1)} = \frac{1}{k^{(j)}} \mathbf{R} \Psi^{(j)}, \qquad j = 0, 1, 2, \dots$$
 (2.15)

In this method, the previous source distribution  $\Psi^{(j)}$  and the multiplication factor  $k^{(j)}$  in generation or cycle j are used to determine the new cycle distribution  $\Psi^{(j+1)}$ . To obtain the new  $k^{(j+1)}$ , the following estimation can be employed:

$$k^{(j+1)} = \frac{N_F^{(j)}}{N^{(j)}} = \frac{\left\langle \mathbf{R}\Psi^{(j+1)} \right\rangle}{\left\langle \mathbf{R}\Psi^{(j)} \right\rangle} = \frac{\left\langle \mathbf{R}\Psi^{(j+1)} \right\rangle}{k^{(j)} \langle \Psi^{(j+1)} \rangle}$$
(2.16)

where  $N_F^{(j)}$  is the total number of neutrons created by fission at j-th iteration,  $N^{(j)}$  is the total number of neutrons starting at j-th iteration, and the  $\langle \cdot \rangle$  notation denotes the integration over all independent variables. It is important to note that an initial guess for k and  $\Psi$ , namely  $k^{(0)}$  and  $\Psi^{(0)}$ , must be provided for the standard power iteration method. The fundamental eigenfunction and eigenvalue can be obtained with an arbitrary initial guess due to the convergence behaviour of this method. To begin with, the recursive substation of Eq. (2.15) is performed:

$$\Psi^{(1)} = \frac{1}{k^{(0)}} \mathbf{R} \Psi^{(0)}$$
 
$$\Psi^{(2)} = \frac{1}{k^{(1)}} \mathbf{R} \Psi^{(1)} = \frac{1}{k^{(0)} k^{(1)}} \mathbf{R}^2 \Psi^{(0)}$$
 :

$$\Psi^{(j)} = \frac{1}{\prod_{m=0}^{j-1} k^{(m)}} \mathbf{R}^{j} \Psi^{(0)}$$
(2.17)

By expressing  $\Psi^{(0)}$  in terms of its eigenmodes:

$$\Psi^{(0)} = \sum_{i=0}^{\infty} a_i \Psi_i \tag{2.18}$$

and substituting Eq. (2.18) into Eq. (2.17), we obtain:

$$\Psi^{(j)} = \frac{1}{\prod_{m=0}^{j-1} k^{(m)}} \mathbf{R}^{j} \left( \sum_{i=0}^{\infty} a_{i} \Psi_{i} \right) = \sum_{i=0}^{\infty} \frac{a_{i}}{\prod_{m=0}^{j-1} k^{(m)}} \mathbf{R}^{j} \Psi_{i}$$
(2.19)

Similar to Eq. (2.12), for each eigenfunction,

$$\Psi_i = \frac{1}{k_i} \mathbf{R} \Psi_i \quad \text{or} \quad \mathbf{R} \Psi_i = k_i \Psi_i$$
 (2.20)

Substituting Eq. (2.20) into Eq. (2.19) results in:

$$\Psi^{(j)} = \sum_{i=0}^{\infty} \frac{a_i}{b} k_i^j \Psi_i \tag{2.21}$$

where  $b = \prod_{m=0}^{n-1} k^{(m)}$ . Dividing Eq. (2.21) by  $k_0^j$  results in:

$$\frac{\Psi^{(j)}}{k_0^j} = \frac{a_0}{b} \Psi_0 + \frac{a_0}{b} \left(\frac{k_1}{k_0}\right)^j \Psi_0 + \frac{a_0}{b} \left(\frac{k_2}{k_0}\right)^j \Psi_2 + \cdots$$
(2.22)

Additionally, dividing Eq. (2.14) by  $k_0$  yields:

$$1 > \left| \frac{k_1}{k_0} \right| > \left| \frac{k_2}{k_0} \right| > \dots \tag{2.23}$$

Eq. (2.22) suggests that if the iteration j is sufficiently large,  $\Psi^{(j)}$  will eventually converges to  $\Psi_0$ . The ratio  $|k_1/k_0|$  represents the largest term in the series, as indicated by Eq. (2.23), implying that the convergence behaviour depends on the value of this ratio. This ratio is known as the dominance ratio ( $\rho$ ). The closer the  $\rho$  value to unity, the slower the convergence to the fundamental eigenfunction. This situation is known as the high dominance ratio problem. Generally, a high dominance ratio system

may require hundreds or thousands of iterations to achieve convergence, while a low dominance ratio system may require tens to hundreds (Brown, 2009).

## 2.2 Nuclear Criticality Calculation

The nuclear criticality problem can be solved using deterministic or probabilistic methods. The deterministic method requires discretizing and solving the neutron transport equation for all variables, such as spatial, angular, and energy, in a deterministic manner (Lewis & Miller, 1984). However, this method encounters drawbacks in terms of computational memory, time, and accuracy when dealing with three-dimensional problems. On the other hand, with the availability of high-performance computers today, the probabilistic method, also known as the Monte Carlo method, can address three-dimensional problems with continuous energy data without discretization errors. However, there are stochastic uncertainties associated with the Monte Carlo method. In this study, only the Monte Carlo method is deployed for all criticality calculations.

# 2.2.1 The Monte Carlo Method

The concept behind the Monte Carlo (MC) method is to derive an outcome from a known probability distribution using random sampling, with a specified number of particles to be sampled (Haghighat, 2021). A simple example illustrating the Monte Carlo method is estimating the value of  $\pi$  (McClarren, 2018). Initially, a circle with a radius of one, centred at the origin, is inscribed within a square with a side length of two, as depicted in Figure 2.1. The ratio of the areas of these two shapes is given by:

$$\frac{\text{Area of the circle}}{\text{Area of the square}} = \frac{\pi(1)^2}{2 \times 2} = \frac{\pi}{4}$$
 (2.24)

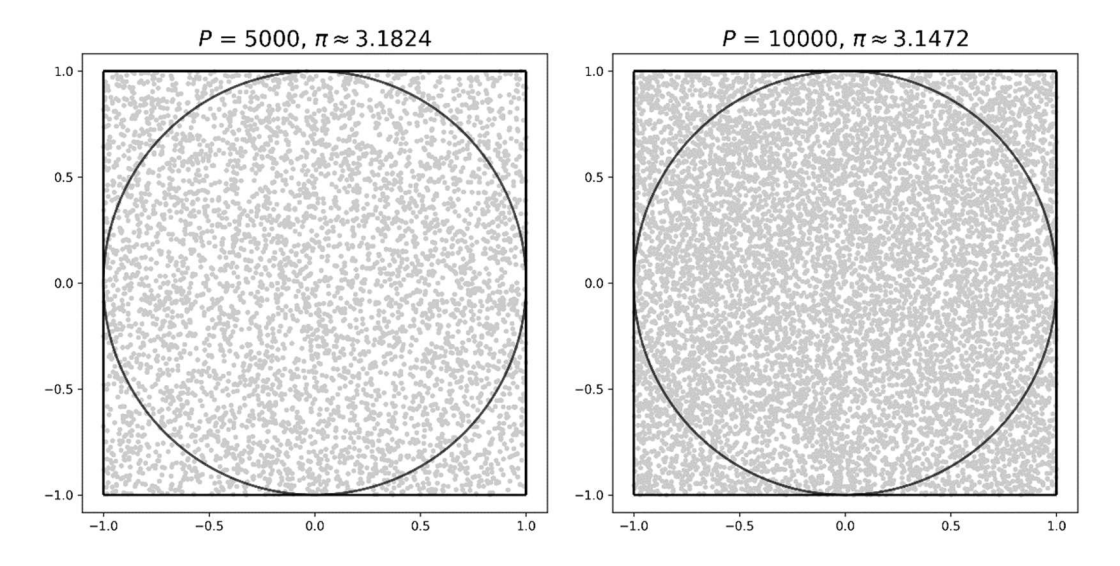


Figure 2.1 The values of  $\pi$  estimated by the Monte Carlo method under different numbers of points P.

Subsequently, a random point with coordinates (x, y) in the domain of [-1, 1) is generated and placed within the square. By dropping a large number of points, the value of  $\pi$  can be estimated from the ratio in Eq. (2.24) using the following formula:

$$\pi = 4 \times C/P \tag{2.25}$$

where C represents the number of points dropped inside the circle and P denotes the total number of dropping points. Note that the random points are generated from a uniform distribution in the interval of [-1,1). As the random numbers are associated with stochastic uncertainty, the simulation must be repeated for multiple MC cycles to assess the uncertainty in terms of variance or standard deviation. The flow chart for the Monte Carlo calculation of  $\pi$  value is presented in Figure 2.2. The first step involves determining the number of particles or points (P) and the number of MC cycles (S) to be simulated. The value of P significantly affects the accuracy of the result, as a low value may introduce significant bias, as illustrated in Figure 2.1. Conversely, a higher value of S can reduce the variance of the results. A pseudorandom number generator is utilized to generate the input points. The sequence

of pseudorandom numbers is initialized using a seed, enabling the replication of simulation results with the same seed. Although the randomness of the sequence may introduce nonuniform random bias, modern algorithms generate pseudorandom numbers that are sufficiently close to true randomness, which minimises this effect. Once all MC cycles are simulated, the mean and standard deviation of the estimated value of  $\pi$  can be calculated.

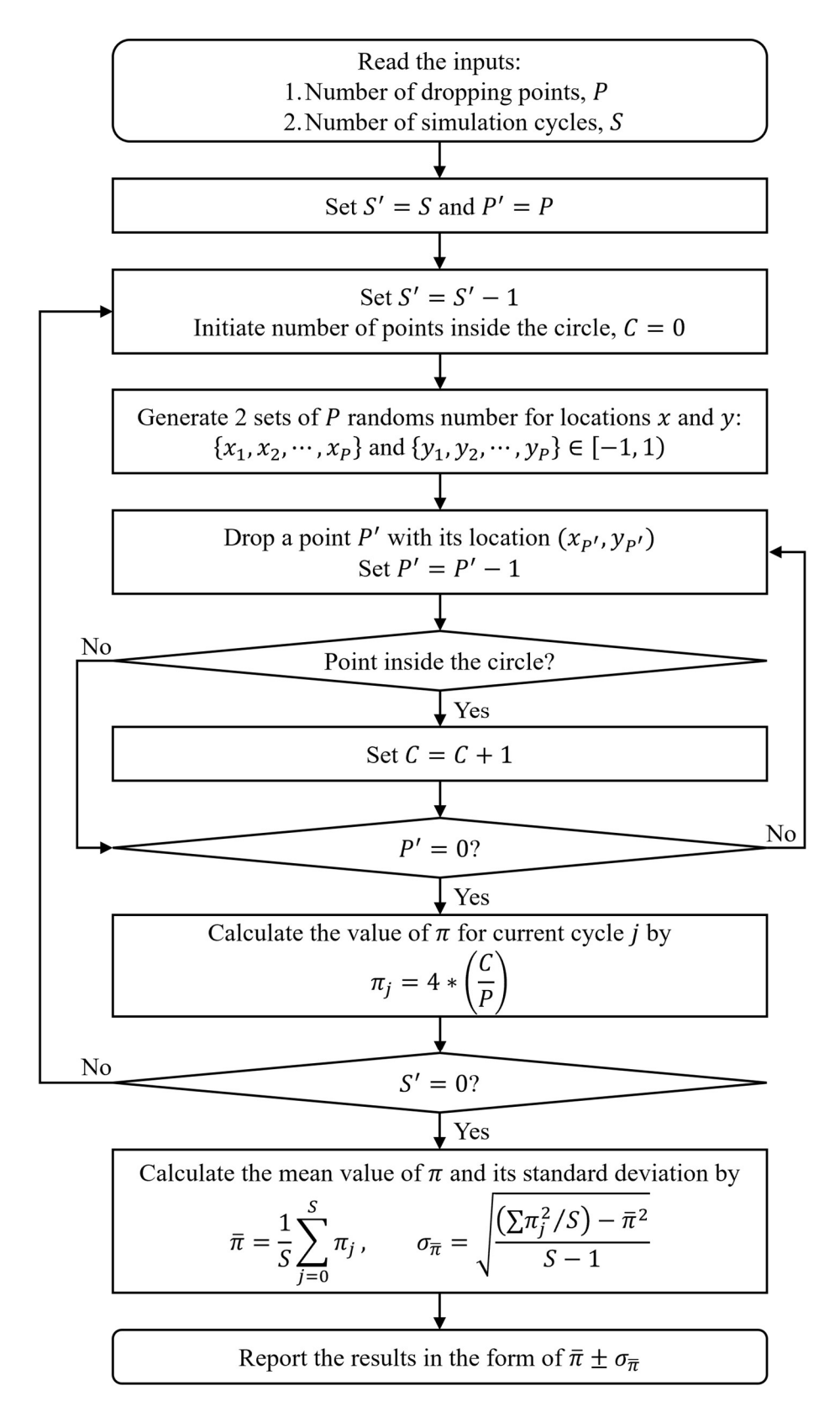


Figure 2.2 The Monte Carlo calculation flowchart for estimating the value of  $\pi$ .

## 2.2.2 Monte Carlo Criticality Calculation

For the nuclear criticality calculation, the Monte Carlo (MC) method does not directly solve the criticality equation. Instead, it simulates the trajectory of each neutron through a random walk from its birth until its termination. All events experienced by the neutron during its journey are recorded. The transport distance and the nature of neutron-nucleus interactions are determined by random sampling from known probability distributions, guided by physical quantities such as material density, material cross sections, and boundary conditions. These probability distributions are derived from experiments and stored in an evaluated nuclear data library. A high-fidelity nuclear data library containing diverse materials is essential to ensure that each simulated neutron adheres to the probability distributions corresponding to actual events.

A large number of neutron histories is necessary for the MC simulation to reduce bias in the  $k_{\rm eff}$  and other interested tallies. Furthermore, a low number of neutron histories used in problems with a high dominance ratio may lead to the occurrence of neutron clustering phenomena (Dumonteil et al., 2014), which can impact the convergence of the fission source (Nowak et al., 2016). Expert recommendation indicates that a minimum of 10,000 neutron histories is required for all calculations (Brown, 2011). In addition, for large and complex geometry problems, such as 3D reactors or storage vaults, it is preferable to use 100,000 or more histories (Brown, 2011).

Another source of bias in the simulation results arises from an inaccurate initial guess of the source distribution. While the MC iteration method will eventually converge the initial distribution to the true distribution, it is crucial to determine

whether the number of inactive MC cycle is sufficient for achieving convergence. The number of inactive cycles depends on the dominance ratio of the problem, the number of neutron histories per cycle, and the initial source distribution. Suppose the initial source guess does not encompass the most important region of the problem and an insufficient number of histories are used. In that case, the dominance ratio of the problem may increase. These two factors make it more challenging for neutrons to propagate towards the true distribution. Hence, the advice from the expert is to employ a uniform distribution as the initial source distribution in all fissionable regions of the problems (Brown, 2011). Furthermore, the number of inactive cycles can be determined by monitoring the convergence trend for around 100 MC cycles, using a moderate number of neutron histories per cycle, such as 1,000. However, this assumes that the convergence behaviour remains unchanged as the number of neutron histories increases. Results from the Massachusetts Institute of Technology (MIT) group (Kumar et al., 2020) indicate that as the number of neutron histories increases, the number of cycles required to reach stationarity also increases.

# 2.3 Source Convergence Indicators

An indicator is necessary to monitor the convergence trend of the fission source distribution in Monte Carlo (MC) criticality problems. Suppose the indicator is a function of the MC cycle. In that case, the number of inactive cycles or the convergence instance can be determined when it reaches a state of stationary or equilibrium. Moreover, certain problems exhibit slow convergence due to a high dominance ratio, thus requiring the indicator to accurately reflect the slow convergence trend. One early attempt at this slow converging problem is the sandwich method (Naito & Yang, 2004), which utilizes two  $k_{\rm eff}$  as convergence indicators. By selecting

two suitable initial source distributions, one with a higher value of  $k_{\rm eff}$  and the other with a lower value of  $k_{\rm eff}$ , the convergence can be assessed by monitoring the monotonically increasing and decreasing behaviours of these two  $k_{\rm eff}$  values. When both values reach a stationary state, then  $k_{\rm eff}$  is converged. However, this method was abandoned as it was discovered that  $k_{\rm eff}$  converges faster than the source distribution (Ueki & Brown, 2003a). Monitoring the source distribution is challenging as it involves a complex function encompassing all source site information. Therefore, various indicators have been proposed from different approaches to represent the source distribution in a simpler manner, which can be divided into two categories: entropy-based indicators and mesh-free indicators.

## 2.3.1 Entropy-Based Indicators

## Shannon Entropy

Shannon entropy is the widely used indicator in most Monte Carlo (MC) codes as it had been adapted as the default source convergence indicator (Kulesza et al., 2022; Leppänen et al., 2015; Romano et al., 2015; Wang et al., 2015). This indicator is adopted from information theory, in which the randomness or disorder of the source distribution is measured (Cover & Thomas, 2005; Ueki & Brown, 2002, 2003b). Users are required to provide a meshing scheme to discretize the problem space. For each MC cycle j, Shannon entropy H can be calculated as:

$$H^{(j)} = -\sum_{i=1}^{B} f_i^{(j)} \log_2 f_i^{(j)}$$
 (2.26)

where  $f_i$  is the neutron source fraction in meshing bin i and B is the total number of meshing bins. It is worth noting that the maximum value of Shannon entropy is  $\log_2 B$  for a uniform distribution, while the minimum value is zero for a point distribution.

The advantage of Shannon entropy is that it condenses the complex neutron distribution into a scalar number for each MC cycle. The choice of meshing scheme is important as it significantly affects the values of Shannon entropy. However, selecting a meshing scheme relies on users' experience with different cases (Kumar et al., 2020; Omar, 2021a; Ueki & Chapman, 2011). For instance, the default meshing scheme in the MCNP code divides the problem space into meshes containing an average of 20 neutron histories per cycle (Kulesza et al., 2022). However, this requirement can impose a computational burden when a vast number of neutron histories are used. On the other hand, an extreme choice where each mesh contains only one neutron history fails to provide the convergence information for the source distribution using Shannon entropy (Cheatham & Brown, 2006; Shi, 2010). Another approach to the meshing scheme is to assign each meshing bin to a different region based on the problem's geometrical configuration. However, this approach does not guarantee accurate convergence results when a large number of neutron histories per mesh are used (Guo et al., 2022; Kumar et al., 2020). Hence, the meshing scheme should be chosen carefully to avoid the wrong determination of source convergence.

Undersampling the neutron population induces neutron clustering, in which neutrons cluster together due to cycle-to-cycle correlations of the fission sources (Dumonteil et al., 2014). Shannon entropy cannot detect the spatial fluctuations of the neutron population resulting from neutron clustering. Therefore, a higher-order spatial moment entropy function has been proposed (Nowak et al., 2016). The entropy function is generalized using Legendre polynomials as follows:

$$S_{u,v,w}^* = -\sum_{i,j,k} L_u(X_i) L_v(Y_j) L_w(Z_k) f_{i,j,k} \log_2(f_{i,j,k})$$
(2.27)

where  $L_q(T)$  represents the Legendre polynomials of order q with argument T and  $(X_i, Y_i, Z_k)$  denotes the x, y, or z-coordinates of the centres of cell i, j, k, normalized

to the interval [-1, 1]. By setting (u, v, w) = (1, 0, 0), the local fluctuations along the x-axis can be monitored using this higher spatial moment entropy. The same applies to  $S_{0,1,0}^*$  and  $S_{0,0,1}^*$ , which monitor local fluctuations along y- and z-axes. However, the impact of neutron clustering on source convergence is still debatable (Mickus & Dufek, 2021).

# Progressive Relative Entropy (PRE)

The alternative version of entropy is progressive relative entropy (PRE), which has been proposed as a convergence diagnostic tool for fission sources (Ueki, 2008b, 2009; Ueki & Brown, 2005). PRE measures the deviation of a source distribution  $S^{(j)}$  from a reference distribution  $S^{(r)}$ , defined as:

$$PRE^{(j)} \equiv D\left(S^{(r)} \parallel 0.5 \times \left(S^{(r)} + S^{(j)}\right)\right) + D\left(S^{(j)} \parallel 0.5 \times \left(S^{(r)} + S^{(j)}\right)\right)$$
(2.28)

Here,  $D(S^{(r)} \parallel S^{(j)})$  represents the relative entropy of  $S^{(r)}$  with respect to  $S^{(j)}$ :

$$D(S^{(r)} \parallel S^{(j)}) \equiv \sum_{i=1}^{B} S_i^{(r)} \log_2 \left(\frac{S_i^{(r)}}{S^{(j)}}\right)$$
 (2.29)

where j is the current MC cycle, r is the reference MC cycle (usually the first cycle),  $S_i$  is the neutron source fraction in meshing bin i, and B is the total number of meshing bins. The formulation of PRE ensures a monotonically increasing trend as the MC cycles progress. This property allows using on-the-fly convergence diagnostic tools such as the Wilcoxon rank sum test to determine the number of inactive cycles. However, similar to Shannon entropy, PRE is also strongly influenced by the refinement of the meshing scheme, thus it faces the same limitations.

## Summary

In a nutshell, the entropy method requires the discretization of the problem space to demonstrate source convergence. Space discretization is crucial in determining the entropy method's efficiency and accuracy (Kumar et al., 2020; Nowak et al., 2016). Therefore, various mesh-free methods have been proposed to ease the cognitive effort in detecting MC simulation convergence.

# 2.3.2 Mesh-Free Indicators

## Source Centre of Mass

The centre of mass of the neutron source has been proposed to diagnose source convergence without employing a meshing scheme (Haghighat, 2021; Wenner, 2010). This method utilizes a single indicator  $|\vec{R}|$  to represent the source distribution in the j-th MC cycle:

$$\left|\vec{R}^{(j)}\right| = \frac{1}{M} \sum_{i=1}^{N} m_i \sqrt{x_i^2 + y_i^2 + z_i^2}$$
 (2.30)

where *i* denotes the neutron index, *m* represents the neutron mass,  $M = \sum_{i=1}^{N} m_i$  is the total mass of all neutrons, *N* indicates the total number of neutrons, and (x, y, z) denotes the magnitude of the vector components from the geometric centre of the model to the *i*-th neutron. However, this indicator encounters an issue when the model and initial source distribution are symmetric. In such cases, the centre of mass will fluctuate around the geometric centre from the initial MC cycle, failing to illustrate the change in source distribution (Guo et al., 2022; Kumar et al., 2020). Besides that, undersampling caused by vacuum boundary conditions may yield inaccurate results (Haghighat, 2021). On the other hand, the components of the centre of mass along each axis have been used to compare with the higher spatial moment expansion of Shannon

entropy, aiding in the illustration of local fluctuations in the neutron population due to neutron clustering (Nowak et al., 2016).

## *Nice-Centre Distance Sum (NCDS)*

The nine centre-distances sum (NCDS) method addresses the limitations of the centre of mass in the case of a symmetric initial source and problem by introducing nine geometric centres at different locations (Ueki & Chapman, 2011). In a 3D problem, the geometry centre of all neutrons is calculated, and then this centre is served as the intersection point for three perpendicular axis planes: the xy, yz, and zx planes. These planes divide the entire problem space into eight subspaces. The geometric centre of source particles within each of the eight subspaces is then computed. The distances between the nine centres in j-th MC cycle and the nine centres in the first cycle are combined into a single indicator D, the NCDS, as follows:

$$D_{xyz}^{(j\to 1)} = \sum_{i=1}^{9} d_{xyz,i}^{(j\to 1)} = \sum_{i=1}^{9} \sqrt{\left(x_i^{(j)} - x_i^{(1)}\right)^2 + \left(y_i^{(j)} - y_i^{(1)}\right)^2 + \left(z_i^{(j)} - z_i^{(1)}\right)^2}$$
(2.31)

where i represents the centre index and  $(x^{(k)}, y^{(k)}, z^{(k)})$  denotes the coordinates of each centre in the k-th MC cycle. Note that for 1D and 2D problems, the NCDS reduces to a sum of three centre-distances or five three centre-distances, respectively. However, the accuracy of this indicator is doubted for certain special symmetric geometries with specific initial source distributions (Guo et al., 2022; Kim et al., 2014). Additionally, automated meshing can be computationally expensive, and implementation of the algorithms may require significant programming efforts (Omar, 2021a).